Comet Interceptor

Dust Hazard Assessment using the Engineering Dust Coma Model (EDCM)

Version 4.2

(Dated: January 21, 2022)

Changelog

v1.0 First version of model

v2.0 Added constraint based on [1] to the scaling model.
Added instruction on how to convert results as a function of dust radius to a function of dust mass.

v2.1 Correction of a scaling error. Addition of figures to the delivery package illustrating the results.

v3.0 Expansion of parameter space to allow for smaller comets with lower activity. Standard case chosen to be compatible with a Halley type comet.

v4.0 Calibration of model to Giotto data. Use of Giotto like trajectory for Giotto comparison instead of S/C B1. Correction of printing error in cometo-centric distance. Slight redefinition of standard input parameters

v4.1 Addition of model sensitivity to changes in the trajectory and empirical scaling laws for changes in CA distance, α_T, and β_T (section V). New figure and explanation describing the different phase curves of 1P and 67P.

v4.2 Addition of interpolation between dust size bins and bin sizes and scaling of the number density with closest approach distance. Explanation of the dust velocities and respective maximum impact angle of the dust with respect to the ram direction of the spacecraft. Addition of mapping of number density to column density.

CONTENTS

I. PURPOSE

Comet Interceptor will pass through a potentially hazardous region of a comet's inner coma. It is therefore important to assess the dust impact risk to the three spacecraft and their science instruments to aid hazard mitigation strategies. The purpose of the Engineering Dust Coma Model (EDCM) is to make predictions of which dust the three spacecraft will encounter during the active phase of the mission. The requirement is to make realistic predictions based on a limited number of input parameters known with large uncertainty and generate a straightforward output, which is provided to industry and to the instrument teams for operational purposes.

II. THE ENGINEERING DUST COMA MODEL

The EDCM is composed of three blocks (models):

- *dust dynamical* model that calculates the spatial distribution of dust,
- *scaling* model that determines the absolute scaling of the dust densities,
- *instrument* model that extracts the number density encountered along the spacecraft trajectories and performs the probabilistic calculations.

Those blocks are depicted in magenta, blue, and green, respectively in Fig. 1.
The inputs parameters required by the dust dynamical model and the scaling model, together with the available parameter ranges, are listed in Table I, whereas the parameters used are listed in Table II. We have chosen not to use the full range of the available parameter space because we wanted the EDCM to reflect for the moment a Halley like comet. But should there be a desire in the future to use the EDCM for other purposes with different assumptions then this can be implemented within the full parameter space shown in Table I. Figure 1 also illustrates which parameters are required by which model.

Two principles lead us to selected parameter ranges. First, we wanted to cover the largest plausible range for each of the parameters. The large ranges for some parameters thus reflect the uncertainty in our knowledge about the future target of CI. Second, because these parameters are inter-dependent and thus cannot be chosen arbitrarily and independently

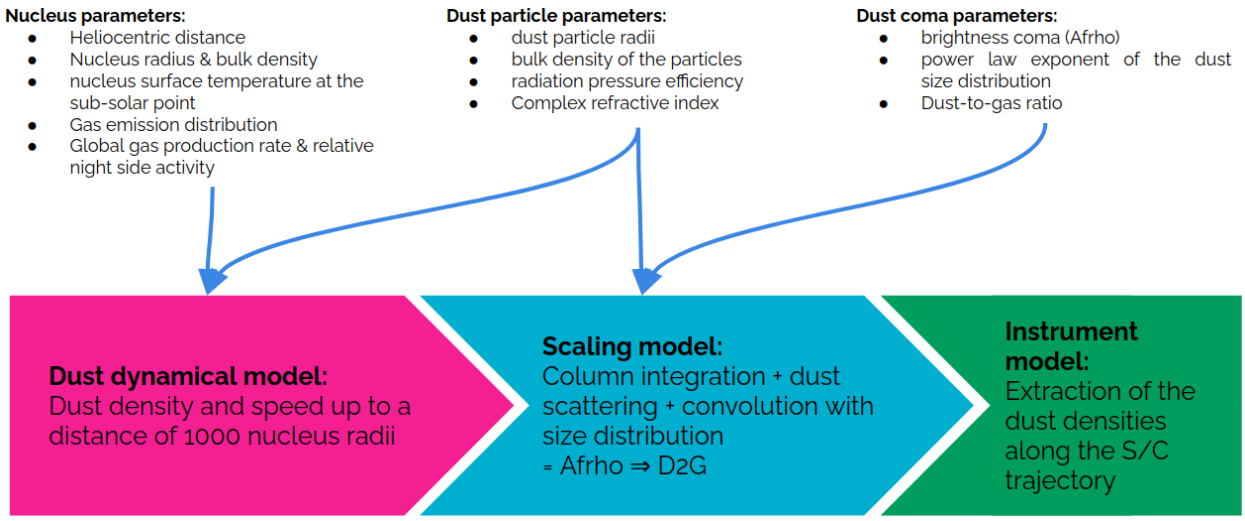

FIG. 1. Sketch of the EDCM and its inputs.

from each other we required the ranges to be consistent with each other. For example, a very steep power law in conjunction with a very high Afρ could result in a unrealistically high χ (100 or higher). Such combinations would be rejected as valid solutions. Figure 2 illustrates this by showing χ as a function of the power law exponent for a large number of input parameters assuming that Afρ = 100 cm. Parameter combinations where $\chi > 10$ (shaded red area) are excluded in the final analysis.

A. Dust dynamical model

The dust dynamical model describes the dust distribution within a cometary coma up to 1000 nuclues radii (R_N). It uses minimal number of parameters for the description of a cometary dust coma, while keeping it physically realistic. This model physically consistently takes into account the expanding nature and asymmetry of the gas coma (caused by gas production modulated by solar radiation) and considers the dust dynamics driven by the gas drag force, force from the nucleus gravity, and solar radiation pressure.

A series of general assumptions were made to simplify the model. For each of the simplifications we have also outlined the resulting limitations that need to be appreciated.

- **The nucleus shape is assumed to be spherical.** The dust dynamical model can therefore not reproduce possible inhomogeneities within the coma that arise due to topography (and often occurs only at particular orientation of the nucleus with respect to the

TABLE I. List of parameters available in the EDCM.

symbol	unit	parameter	value/range/function	step size
		Nucleus parameters		
r_h	au	heliocentric distance	1	n/a
R_N	km	nucleus radius	1, 2, 5-35	5
ρ_N	kg m^{-3}	bulk density of the nucleus	317, 328, 401, 446, 508, 564, 642	n/a
T_N	K	nucleus surface temperature at the sub-solar point	317	n/a
$q(\varphi)$	-	gas emission distribution ($\sim cos^k(\varphi)$)	$k = 1, 2, 3$	n/a
Q_g^{equiv}	s^{-1}	global gas production rate for an equivalent sphere with $R = 1$ km ($Q_g^{equiv} = Q_g/R_N^2$)	$5 \cdot 10^{25} - 4 \cdot 10^{27}$	uniformly sampled
$q_g^{180^\circ}/q_g^{0^\circ}$	-	relative night side activity	0.01, 0.05, 0.1	n/a
		Dust particle parameters		
a	m	radius	$10^{-6} - 10^{-1}$	half decade
$\varrho_d(a)$	kg m^{-3}	bulk density	$300 - 1000$	100
$q_{rad}(a)$	-	radiation pressure efficiency	$0.3 - 2$	~ 0.1
$q_{sca}(a)$	-	scattering efficiency	silicates & organics*	n/a
$\phi(\alpha)$	-	phase function	silicates & organics*	n/a
		Dust coma parameters		
Afρ	cm	brightness	$100 - 100,000$	900
β	-	differential power law exponent of the dust size distribution; $n \sim a^{-\beta}$	$3.6 - 4.4$	0.2
χ^*	-	dust-to-gas mass production rate ratio	< 10	n/a

Note: * See [2].

Sun). Nevertheless, when the parameters of the coma of a complex shape nucleus are averaged over a full comet rotation the resulting average coma distribution resembles closely the one from a spherical nucleus.

TABLE II. List of parameters used in the current version of the EDCM.

symbol	unit	parameter	value/range/function	step size
		Nucleus parameters		
r_h	au	heliocentric distance	1	n/a
R_N	km	nucleus radius	2, 5, 10	n/a
ρ_N	kg m^{-3}	bulk density of the nucleus	317, 508	n/a
T_N	K	nucleus surface temperature at the sub-solar point	317	n/a
$q(\varphi)$	-	gas emission distribution ($\sim cos^k(\varphi)$)	$k = 1, 2, 3$	n/a
Q_g^{equiv}	s^{-1}	global gas production rate for an equivalent sphere with $R = 1$ km ($Q_g^{equiv} = Q_g/R_N^2$)	$1.3 \cdot 10^{27}$ $-4.9 \cdot 10^{28}$	uniformly sampled
$q_g^{180^\circ}/q_g^{0^\circ}$	-	relative night side activity	0.01, 0.05, 0.1	n/a
		Dust particle parameters		
a	m	radius	$10^{-6} - 10^{-1}$	half decade
$\varrho_d(a)$	kg m^{-3}	bulk density	$300 - 1000$	100
$q_{rad}(a)$	-	radiation pressure efficiency	$0.3 - 2$	~ 0.1
$q_{sca}(a)$	-	scattering efficiency	silicates & organics*	n/a
$\phi(\alpha)$	-	phase function	silicates & organics*	n/a
		Dust coma parameters		
Afρ	cm	brightness	$2,800 - 28,000$	2,000
β	-	differential power law exponent of the dust size distribution; $n \sim a^{-\beta}$	$3.2 - 4.4$	0.2
χ^*	-	dust-to-gas mass production rate ratio	< 10	n/a

Note: * See [2].

- **The gas is assumed to be an ideal perfect gas.** The gas flow in the coma is described by the gas-dynamic Euler equations which express the conservation of the mass, momentum and energy in the flow of an ideal perfect gas.

  In other words these equations describe the motion of an equilibrium fluid flow without viscous dissipation and heat conductivity. The real atmosphere of a comet contains

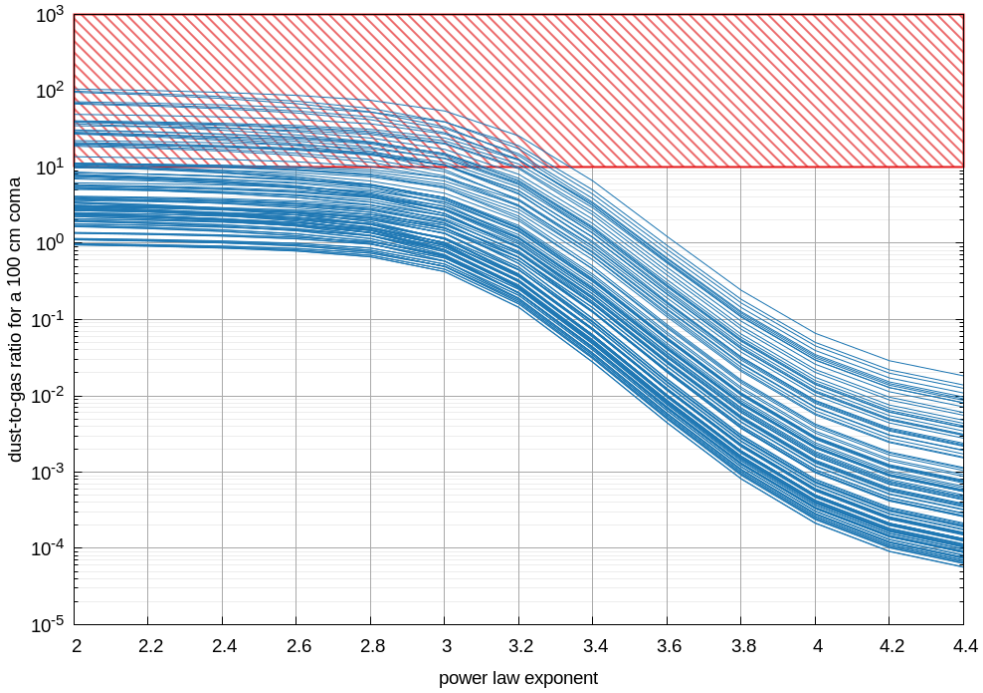

FIG. 2. Dust-to-gas ratio as a function of the power law exponent assuming a dust coma with Afρ = 100 cm.

rarefied non-equilibrium regions as well.

The transfer of thermal energy into kinetic energy in a rarefied flow is less efficient than in a fluid flow, therefore the rarefied flow accelerates slower. Due to the presence of viscous dissipation flow structures like shocks are diffused in a rarefied flow.

Nevertheless, as was shown in many publications, the description of the flow based on the fluid equations preserves general physical realism of the flow.

An important merit of the Euler equations is that they don't depend on the flow rarefaction and therefore the solutions can be scaled for different production rates, the main reason why we use them in the present model.

- **It is assumed that the dust does not influence the gas flow** (i.e. no back-coupling of the dust to the gas flow). This allows the separate/sequential determination of the gas and dust flows. This is given for comets with low dust-to-gas ratios [$\sim<$ 10]. Nevertheless, for a comet with a high dust-to-gas ratio the model will be able to produce reliable predictions.

- **It is assumed that the gas coma is constituted of one single species, H_2O.** This

assumption will be reasonable well satisfied for comets where H_2O is the dominant gas species (as e.g. for comet 67P).

- **It is assumed that there is no extended gas/dust source/sink in the coma.** The model should not be applied to comets with a significant extended gas/dust source/sink e.g. emission of gas from dust particles within the coma, sublimation and destruction of dust particles etc.

- **It is assumed that the gas and dust emission is smooth across the surface or that any inhomogeneities are blurred within the drag acceleration region $r \leq 10R_N$.** The gas and dust emission is modulated e.g. by solar zenith angle. It means that the emission **is not** dominated by a few very localised jets.

- **The model is reliable for cometo-centric distances of $10R_N < r < 1000R_n$.** The low limit is defined by the possible existence of 'fine structure' of the flow due to particularities of the surface structure. The upper limit is defined by the size of computational region. It is possible to extrapolate the data beyond this upper limit via introducing additional assumptions (e.g. sphericity of expansion etc.).

- **The model is run for a heliocentric distance of** 1 AU, the approximate distance of CI's comet during the encounter. Result shall thus not be attempted to be scaled to vastly different heliocentric distances. The results remain valid for variations of the heliocentric distance that do not change the solar flux to the nucleus surface by more than a factor of 2 (i.e. the model is valid for the heliocentric distance range of CI).

- **It is assumed that dust particles are spherical, homogeneous with invariable size and mass.**

For the underlying gas dynamics model we used the results by [3] who have calculated the gas field by solving the Euler equations. The emission distribution at the surface is assumed to be proportional to $cos^k(\varphi)$, where φ is the solar zenith angle, and the power k takes the values 1, 2, and 3 (which corresponds to the different mechanisms of gas production from the nucleus). Nigh-side activity is introduced as uniform emission with respect to φ and quantified by the ratio of the gas production rate at the anti-solar point to the production rate at the sub-solar point, $q_g^{180^\circ}/q_g^{0^\circ}$.

The gas results are used to calculate the dynamics of spherical dust particles taking into account gas drag, nucleus gravity, and solar radiation pressure. An important implicit assumptions to reiterate is that we assume that the dust does not have a back reaction effect on the gas flow. The dust dynamics makes use of dimensionless variables (derived by combining various physical parameters from Table I) to parametrise the dust dynamics as described in [4] and reduce the number of numerical solutions. The result of this step is the dust number density and velocity in 3D space. At this point there is also the implicit assumption that the dust-to-gas mass production rate ratio, χ, is unity. These solutions therefore do not yet have an absolute scale. This is determined in the next step.

B. Scaling model

To determine the absolute scaling of the dust densities we chose to determine χ by calculating Afρ for each set of parameters following the approach described in [5]. The dust column density of an aperture of $20R_N$ is calculated. For points outside the simulation domain ($1000R_N$) a $1/r^2$ extrapolation is applied. The column densities are then convolved with a power law ($n \sim a^{-\beta}$) and converted into reflectance using the scattering model of [6] as shown in [?]. The reflectance can then be used to calculate the Afρ as explained in [7]. The absolute scaling χ can then be determined by linearly scaling the model Afρ to the desired Afρ. I.e. if the model Afρ = 100 cm then an actual coma with Afρ = 200 cm is achieved with $\chi = 2$.

For version 2.0 and higher we added a constraint to the scaling model based on observations of Afρ/Q_{H_2O}. Figure 3 shows the ranges for typical (yellow) and depleted (orange) comets according to Table VI in [1]. The range of the EDCM converse the range of the parameters in Table II. As illustrated in Fig. 3 this results in a much larger range than observed and thus includes much dustier and gassier comets than reported in [1]. For version 2.0 we have therefore constrained the range to $-29.7 <$Afρ/$Q_{H_2O} < -27.65$. This corresponds to a ranges in [1, 8], and Schleicher & Bair (private communication; Oort cloud comets).

For version 4.0 and higher we have chosen to calibrate the model on the Giotto data for a Giotto like fly-by (CA = 600 km and phase at CA = 30 degrees). See section IV for the comparison. The phase functions of 1P and 67P differ significantly, especially at large phase

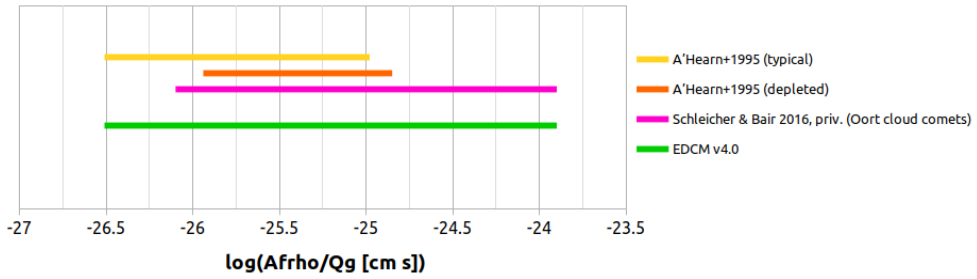

FIG. 3. Shows the log(Afρ/Q$_{H_2O}$) from [1] for typical (yellow) and depleted (orange) comets as well as the ranges of the two versions of the EDCM.

angles (Fig. 4).

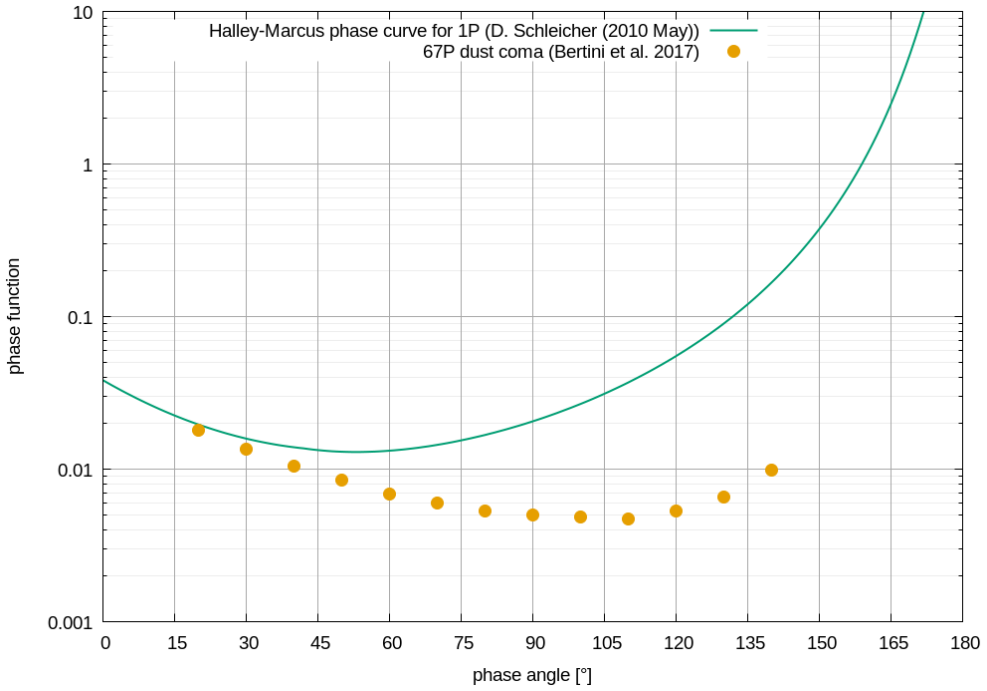

FIG. 4. The phase curves of 1P (Schleicher) and 67P [9] are shown.

Because we employ the scattering model by [6] (which has been calibrated to the 67P phase function) for the calculation of the model Afρ, a global scaling factor is applied to bring in line the measurements at 1P of the Afρ and Giotto dust densities. Therefore, by definition our model fits the Halley data when the appropriate input parameters for Halley are chosen. Thus all results can be understood as relative to Halley. In this sense if the model is applied to e.g. a comet that is otherwise identical to Halley but has a dust to gas ratio that is double that of Halley, the model will predict densities that are double those

measured with Giotto.

C. Instrument model

As last step, having determined the absolute scaling, χ, we extract the number density encountered along the spacecraft trajectories for each combination within parameters space. Again, for points outside the simulation domain ($1000R_N$) a $1/r^2$ extrapolation is applied.

III. EDCM RESULTS

The different values for the input parameters listed in Table II result in $\sim 3,000$ combinations (i.e. possible cases of the dust coma). E.g. for each nucleus radius, four different nucleus bulk densities were run; for each of those combinations three different gas emission distributions were run; for each of those combinations three different night side activity levels were run; for each of those combinations twelve different dust size distributions were run; etc.. Combinations were only discared if they violated a specific constraint, e.g. $\chi > 10$.
As described in Sec. II we have extracted for each dust size bin the number of particles encountered along the spacecraft trajectory. For now we have assumed that the fly-bys of all three spacecraft occur in the same plane, cross the Sun-comet line at 90°, go through 0° phase angle, and have CA distances of 1000, 500, and 200 km for spacecrafts A, B1, and B2 respectively (see Table III).

TABLE III. List of the fly-by parameters used.

symbol	unit	parameter	value	step size
$r_{CA,A}$	km	cometocentric distance of spacecraft A at CA	1000	n/a
$r_{CA,B1}$	km	cometocentric distance of spacecraft B1 at CA	500	n/a
$r_{CA,B2}$	km	cometocentric distance of spacecraft B2 at CA	200	n/a
$\alpha_{T,(A/B1/B2)}$	deg	trajectory angle in the meridional plane (α in Fig. 8)	0	n/a
$\beta_{T,(A/B1/B2)}$	deg	trajectory angle in the equatorial plane (β in Fig. 8)	0	n/a

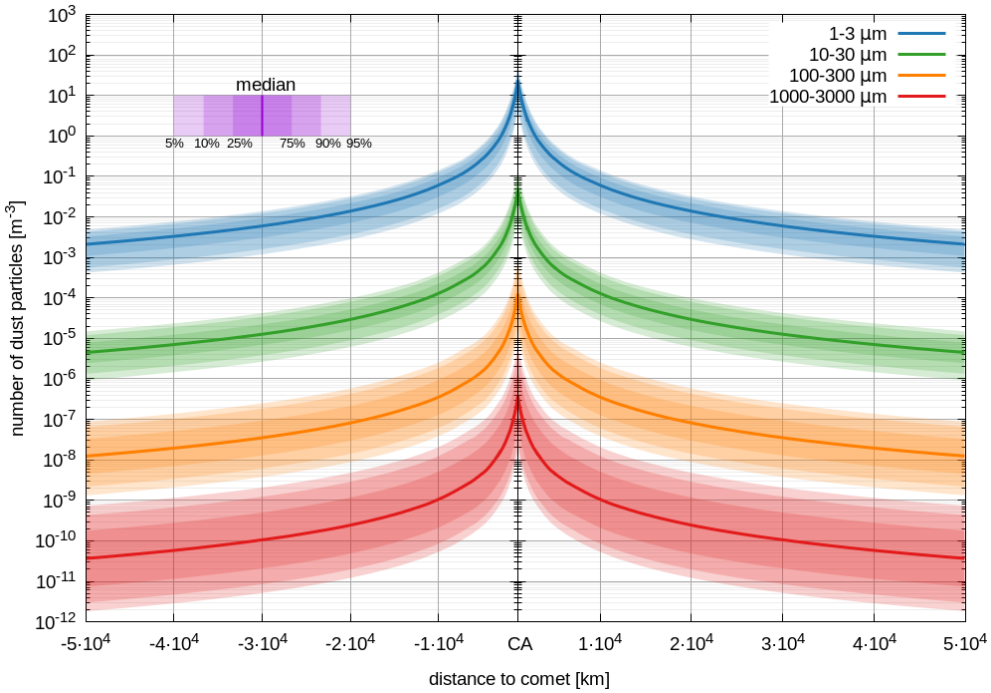

FIG. 5. Number of dust particles according to v4.0 along the spacecraft trajectory of spacecraft A as function of cometo-centric distance. The shaded areas show different percentile ranges within which cases fall.

At each point along the trajectory we calculated the median number of particles predicted by the all model variations as well as the 5^{th}, 10^{th}, 25^{th}, 75^{th}, 90^{th}, and 95^{th} percentile. The results for four size bins is shown in Fig. 5. The shaded areas illustrate the variation in predicted number of particles based on the variation of the input parameters. These ranges thus reflects to a large degree the uncertainty of our knowledge of the future target of CI. As the dust size increases the expected number of particles decreases but the uncertainty increases. Further, the spike in particles around CA highlights that most particles are encountered very close to CA. E.g. from cometo-centric distances of 10,000 km to CA at 1,000 km the dust densities increase by roughly 2.5 orders of magnitude.

We have further integrated the total number of particles per square meter expected along the entire fly-by. The results for spacecraft A are shown in Fig. 6. The figure shows the number of particles per half decade in dust size. This means that the value e.g. given at 1 μm or 3 mm includes the number of particles in the interval from $1-3$ μm or $3-10$ mm respectively. As another example we expect in the median case ~ 1 particle per square meter

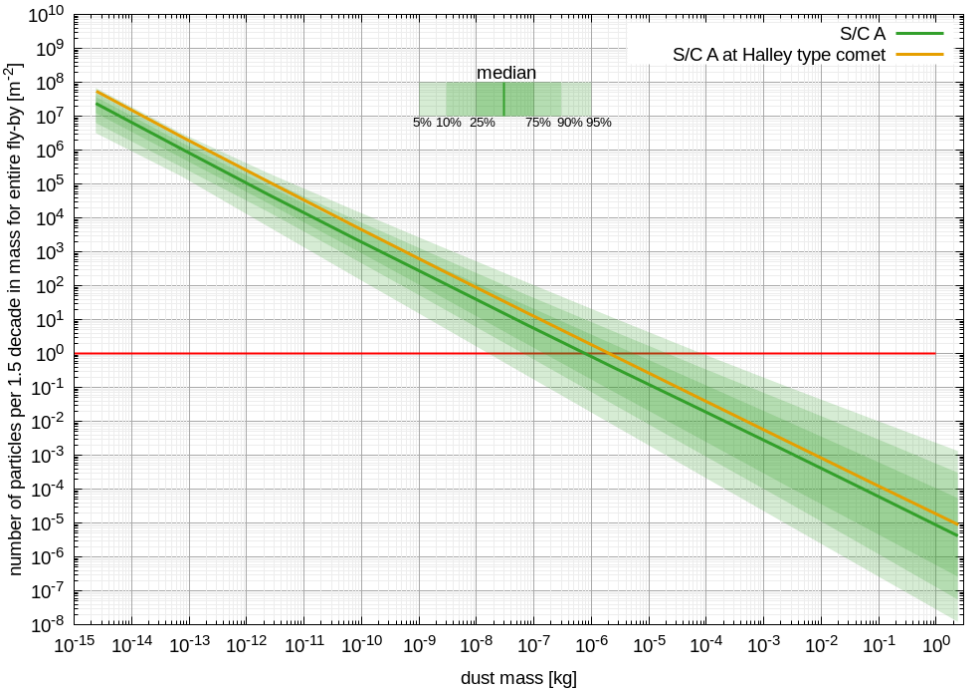

FIG. 6. Total number of dust particles encountered according to v4.0 along the spacecraft trajectory of spacecraft A as function dust mass. The shaded areas show different percentile ranges within which cases fall. Additionally the orange curve shows the predicted median densities for a Halley type comet (according to the definition in Sec. IV).

along the entire fly-by trajectory of spacecraft A in the size range of $300 - 1000$ μm.

Though we do not provide any dust speeds along the different trajectories there are some simple estimates that illustrate that the spacecraft motion with respect to the comet will dominate the flux direction of the dust onto the spacecraft. The terminal dust speeds cannot exceed the gas speed with an upper limit of 1,000 m/s. In the case of isotropic gas expansion from a spherical nucleus the terminal dust velocity, $v_{d,term}$, can be calculated from the approximation of the numerical solution:

$$v_{d,term} = \frac{58.903\sqrt{T_N}}{1 + 0.6\sqrt{1.5/\mathrm{Iv}}} \quad , \tag{1}$$

where

$$\mathrm{Iv} = 4.038 \cdot 10^{-29} \frac{Q_g}{R_N \varrho_d a \sqrt{T_N}} \quad , \tag{2}$$

and where T_N is the nucleus temperature (to be set to 300 K for our purposes here), Q_g is the gas production rate [molecules/s], R_N is the radius of the nucleus [m], and ϱ_d is the bulk

dust density (to be set to the respective value from Tabel VI). The left panel of Fig. 7 shows the terminal dust speeds for the maximum and minimum gas production rates considered in the EDCM. Particles larger than ~ 600 μm are always slower than 100 m/s.

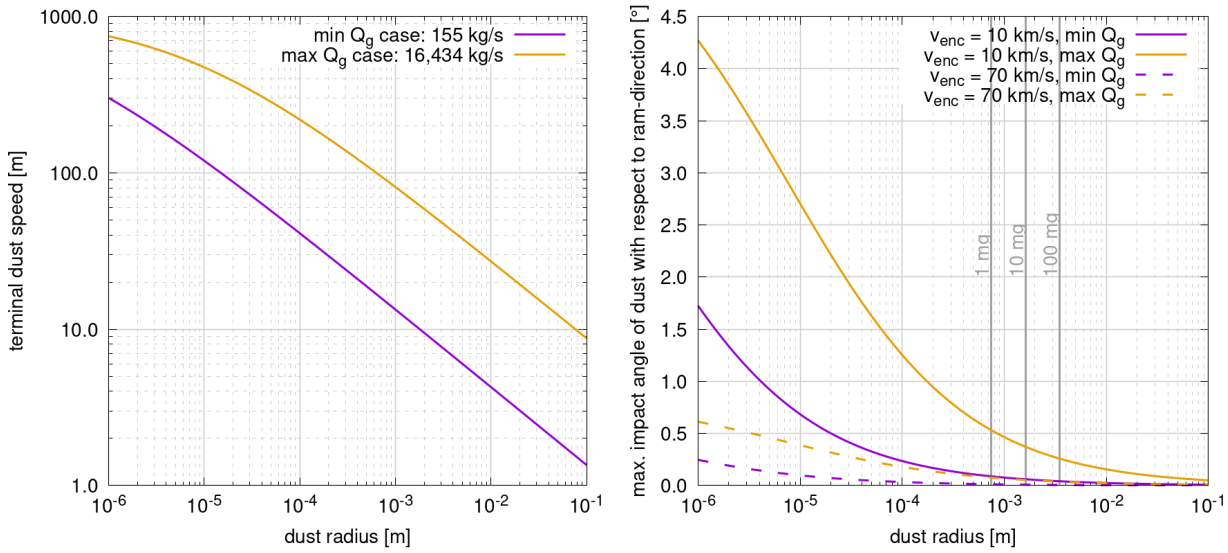

FIG. 7. The left panel shows the terminal dust speed, $v_{d,term}$, according to Eq. 1 for two gas cases. The lowest gas production rate case considered in the EDCM in purple (min Q_g case, where $R_N = 2$ km and $Q_g = 155$ kg/s) and the highest gas production rate case in orange (max Q_g case, where $R_N = 5$ km and $Q_g = 16,434$ kg/s). The right panel shows the maximum angle of impact of dust particles with respect to the ram-direction of the spacecraft. The solid lines are for a fly-by speed of 10 km/s and the dashed lines for 70 km/s. The colours are the min. and max. gas production cases as in the left panel. The corresponding radii of particles with masses 1 mg, 10 mg, and 100 mg are indicated by the grey lines.

From the terminal dust speed we can derive the maximum impact angle of a dust particle with respect to the ram-direction of the spacecraft given a certain fly-by velocity. Currently fly-by velocities between 10 km/s and 70 km/s are considered. The most likely fly-by speed is expected to be 50 km/s. The right panel of Fig. 7 shows this angle which is always smaller than $\sim 0.5°$ for particles with masses larger than 1 mg. The maximum impact angle occurs for the smallest particles (1 μm) in the highest gas production rate case and is $\sim 4.3°$. This illustrates that the impact angles is dominated by the spacecraft fly-by velocity.

Finally, we need to make the reader aware that the percentiles of the number density don't map directly to the respective percentiles of the column densities. For example the

integration of the median number density along the trajectory will not yield the median column density. The reason for this is that there is no global median case i.e. there is no case that provides the median at all cometo-centric distances. Therefore, the median number density is a composite of different cases. In contrast the column density results have a median that can be linked to a "median case". If one e.g. wants to map the median number density to the median column density a correction factor, f, needs to be applied when integrating the number density such that

$$N_{col} = \int f N_{num} dx \quad , \tag{3}$$

where x signifies the integration along the spacecraft trajectory. For the median case of spacecraft B1 and B2 this correction factor is essentially unity for all dust sizes. But for spacecraft A it is $f = 0.53 \pm 0.01$.

IV. EDCM VALIDATION ON EXISTING DATA

The reliability of the EDCM predictions is checked via comparisons with available data of previous missions to comets: Rosetta and Giotto.

The 3-dimensional shape of the comet Halley's nucleus was derived from the combination of Vega and Giotto images. A self-consistent model has been produced using an ellipsoid with 8.0, 8.2, and 16 km for the three axes [10]. A surface is about 400 km^2 and volume of 580 km^3. The spin vector points about 60° south of the comet to sun direction and it is about perpendicular to the long axis of the nucleus. A spin period of 54±1 h matches the data from the three spacecraft.

In situ measurements [11] showed a total gas production rate of 6.9×10^{29} molecules s^{-1} with the predominance of water vapour ∼80% (and 20% more volatile compounds) by volume and the photodestruction scale length for H_2O of 3.9×10^4 km. In [12] was noted that the Halley Multicolour Camera (HMC) images have revealed that the activity of comet Halley's nucleus was concentrated towards the sun and that the variability of the comet during Multi Detector Mode was seen to be small (the minimum-maximum variation is considerably less than a factor of 2).

The results of analysis in [13] provide the mass of the nucleus 1.3±0.3 – 3.1±0.4 $\times 10^{14}$ kg, the mean density of the nucleus 280±100 – 650±190 kg/m^3, and the dust-to-gas ratio 0.3–1.

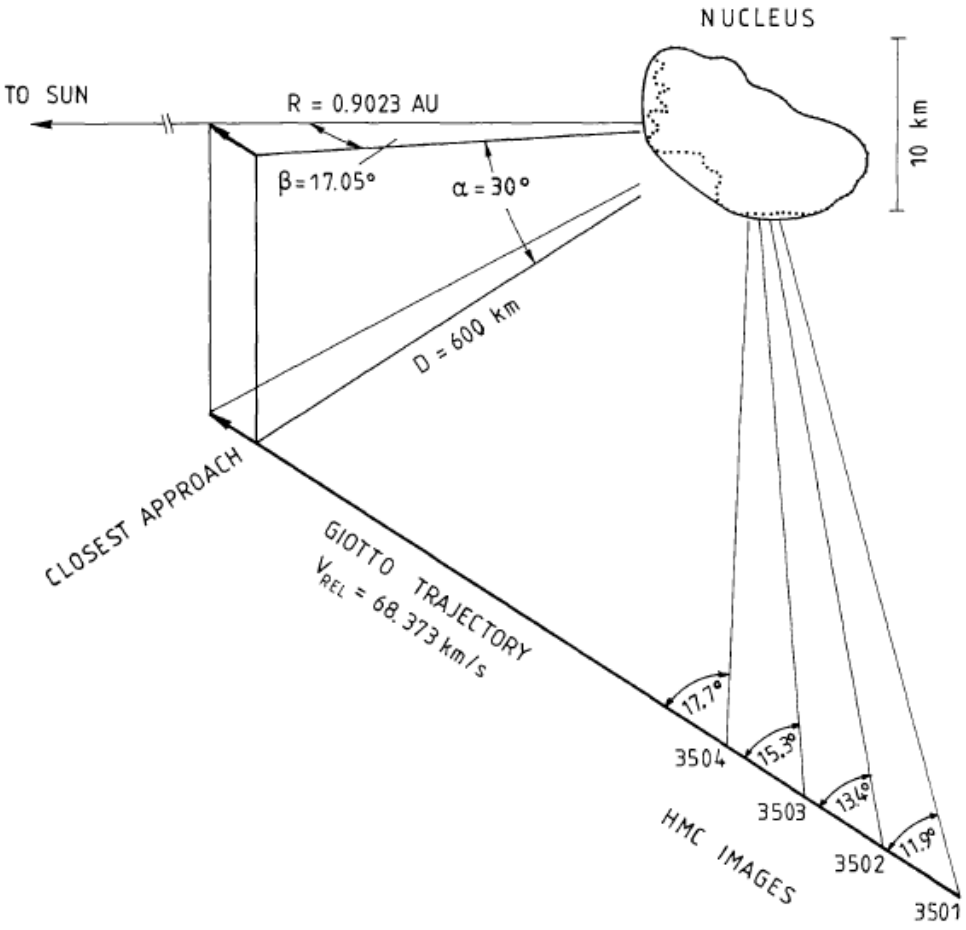

FIG. 8. The Giotto flyby trajectory relative to the cometary nucleus and sin is shown, including offset angles and positions for the last 4 useful HMC images (from [12]).

The EDCM uses axially-symmetric numerical solutions. Therefore, some trajectories which are different in 3D space might be identical in the axially-symmetric frame. The computational frame is shown in Fig. 9. The frame is axially-symmetric with respect to the axis X. Axis +X is directed towards the Sun. R is the distance (i.e. the radius which is always positive) from axis X to some (anyone) point of the trajectory (it is assumed that the trajectory is a straight line). Axis $\vec{Z}$ is a vector product $\vec{X} \times \vec{R}$. Therefore, the trajectory in this frame is given by: the position of the point (X,R) and three direction cosines $(v_x/|v|, v_R/|v|, v_z/|v|)$.

For the model with a spherical nucleus we use the radius of 5 km, a nucleus mass of 2.7×10^{14} kg, the total gas production rate $(5.1\text{-}5.5)\times10^{29}$ s^{-1}, and Afρ of 28,000 cm. The other parameters have been left as free parameters which results in 84 parameter variations. A Giotto like trajectory (CA = 600 km and phase at CA = 30 degrees) has been used. The

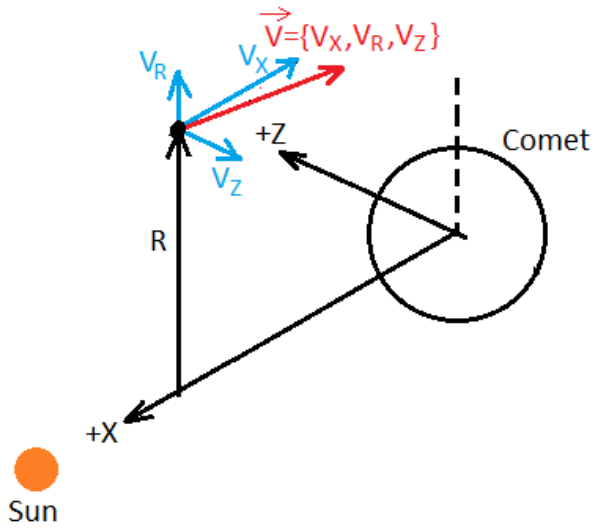

FIG. 9. The frame of the EDCM simulations.

results can be seen in Fig. 10.

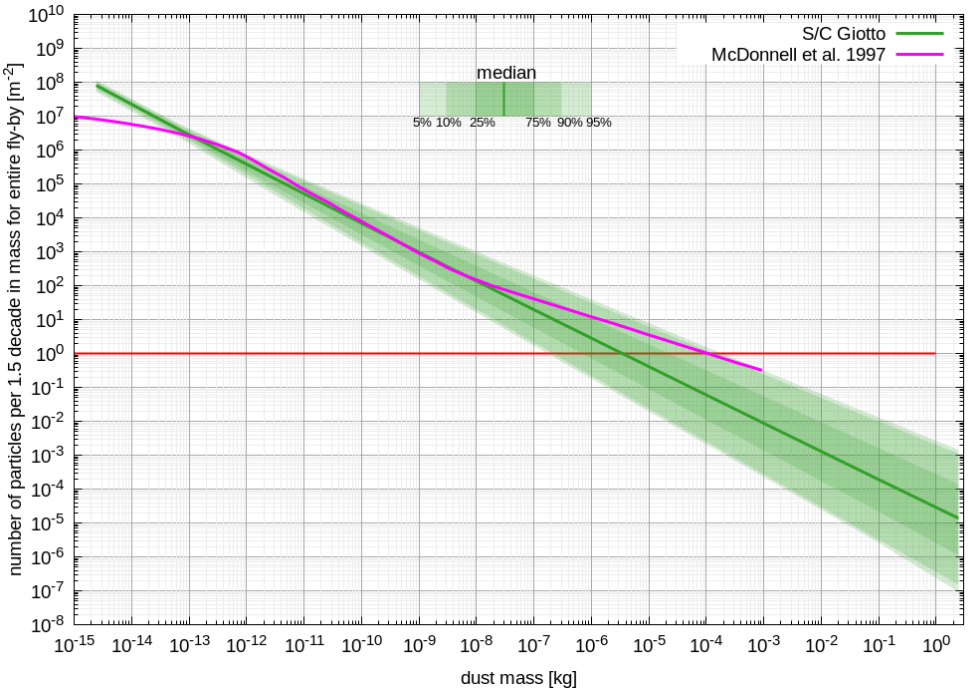

FIG. 10. Total number of particles during encounter as a function of mass for the EDCM Halley case and the data by [14]

The data below 10^{-12} kg is an lower limit measurement and should thus not be considered in the comparison. Apart from that the data lies within the confidence interval of the model

for most of the mass range. In the mass range from 10^{-12} to 10^{-8} kg the model matches well the slope of the Giotto data. Because the size distribution for Halley has a break at $\sim 3 \times 10^{-8}$ or model cannot match that behaviour as it assumes an unbroken power law. But such a power law is implicitly contained in the model because a variety of slopes are simulated with are reflected in the uncertainty.

V. SENSITIVITY TO CHANGES IN THE TRAJECTORY

The nominal trajectories (table III) of the model only vary in CA distance but not in the two angles α_T and β_T (α and β in Fig. 8) which are both assumed to be zero. Because this will not be the case for all three spacecrafts we have tested the model to the sensitivity of changes in α_T, β_T, as well as the CA distance, r_{CA}.

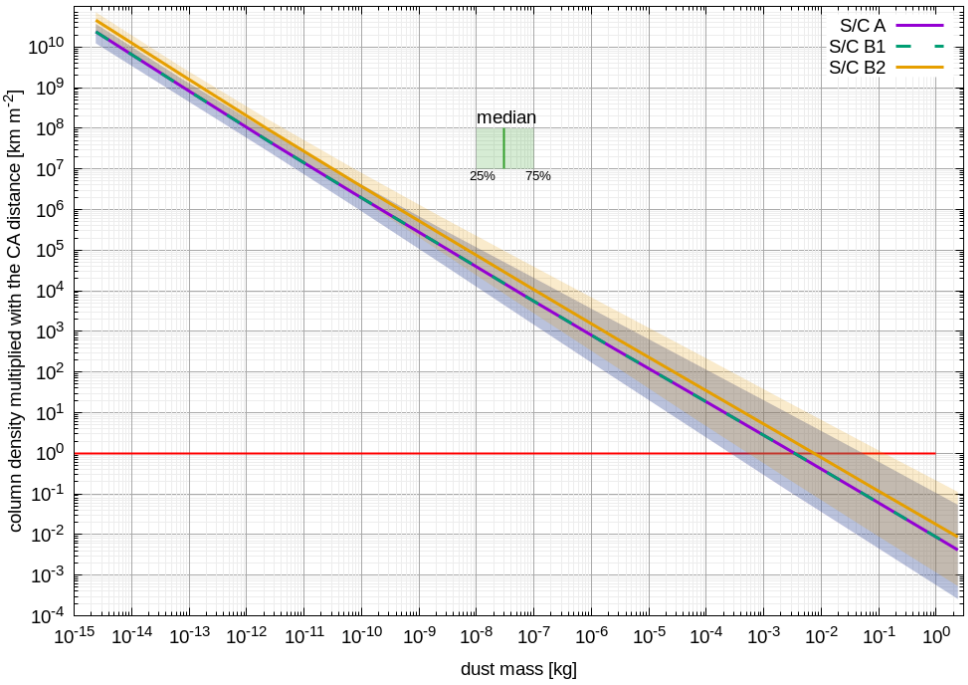

FIG. 11. Column density multiplied with the CA distance as a function of dust mass.

First, we explored variations in the CA distance. For a force free, radially expanding coma the column density scales with 1/CA. Or put another way the product of the column density and the CA distance is constant. Fig. 11 shows this for the three S/C and reveals that this scaling works well for S/C A & B1 but not perfectly for S/C B2 which results in densities roughly a factor of 2 higher than expected from that scaling of the other two S/C. This is

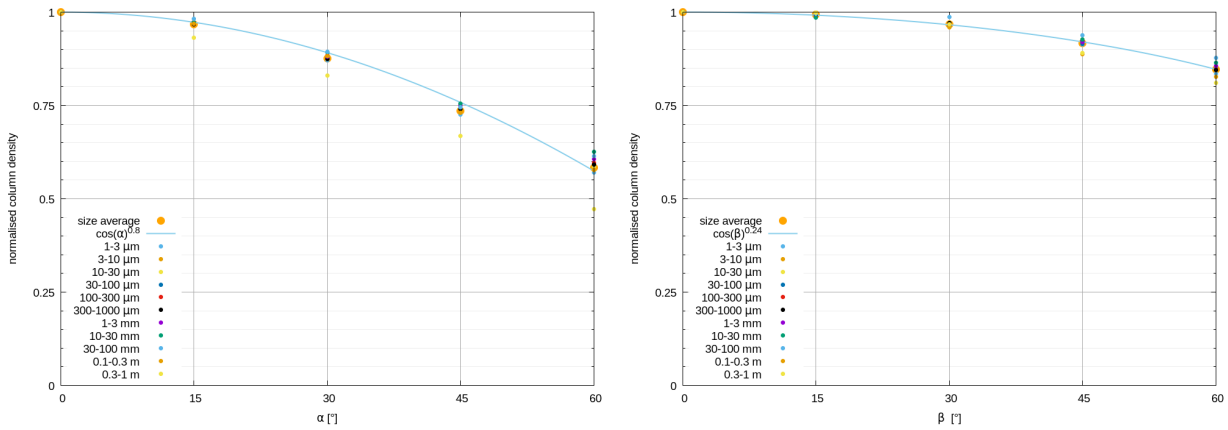

(a) normalised column density as a function of α_T (°) (b) normalised column density as a function of β_T (°)

FIG. 12. Dependence of the column density with α_T and β_T

likely due to the fact that S/C B2 gets very close to the nucleus (down to $20R_N$ in some of the cases considered). In a sense S/C B1 is the nominal case as it is not too close to the nucleus and not too far from the nucleus (where we need to extrapolate the dust results from our modelling domain and thus "force" a 1/CA behaviour). The medians of the different S/C are all still within the centre 50 percentiles of the cases. Thus the uncertainty from the unknown parameters of the model is much larger than the uncertainty of this simple scaling. Also the assumed differences compared here are very large, therefore for small changes in the CA distance the results of the model can be scaled with

$$N_{col}(r_{CA}) = N_{col}(r_{CA;0})\frac{r_{CA;0}}{r_{CA}} \quad , \tag{4}$$

where $r_{CA;0}$ is the reference CA distance. The number densities, N_{num}, scale respectively with the square of the closest approach distance, i.e.

$$N_{num}(r_{CA}) = N_{num}(r_{CA;0})\left(\frac{r_{CA;0}}{r_{CA}}\right)^2 \quad . \tag{5}$$

Next we explore changes in α_T (α in Fig. 8). Changes to only α_T ($\beta_T = 0°$) merely change the phase angle at CA but retain a symmetric trajectory around CA. We've run the EDCM for $\alpha_T = 0°, 15°, 30°, 45°, 60°$ for S/C B2. Figure 12 a) shows the normalised column density to the values of each dust sizes column density at $\alpha_T = 0°$ as well as the size averaged relative column density. The column densities scale roughly as a function of the cosine but barely reach a factor of 2 decrease at $\alpha_T = 60°$ which again is much less than the uncertainties

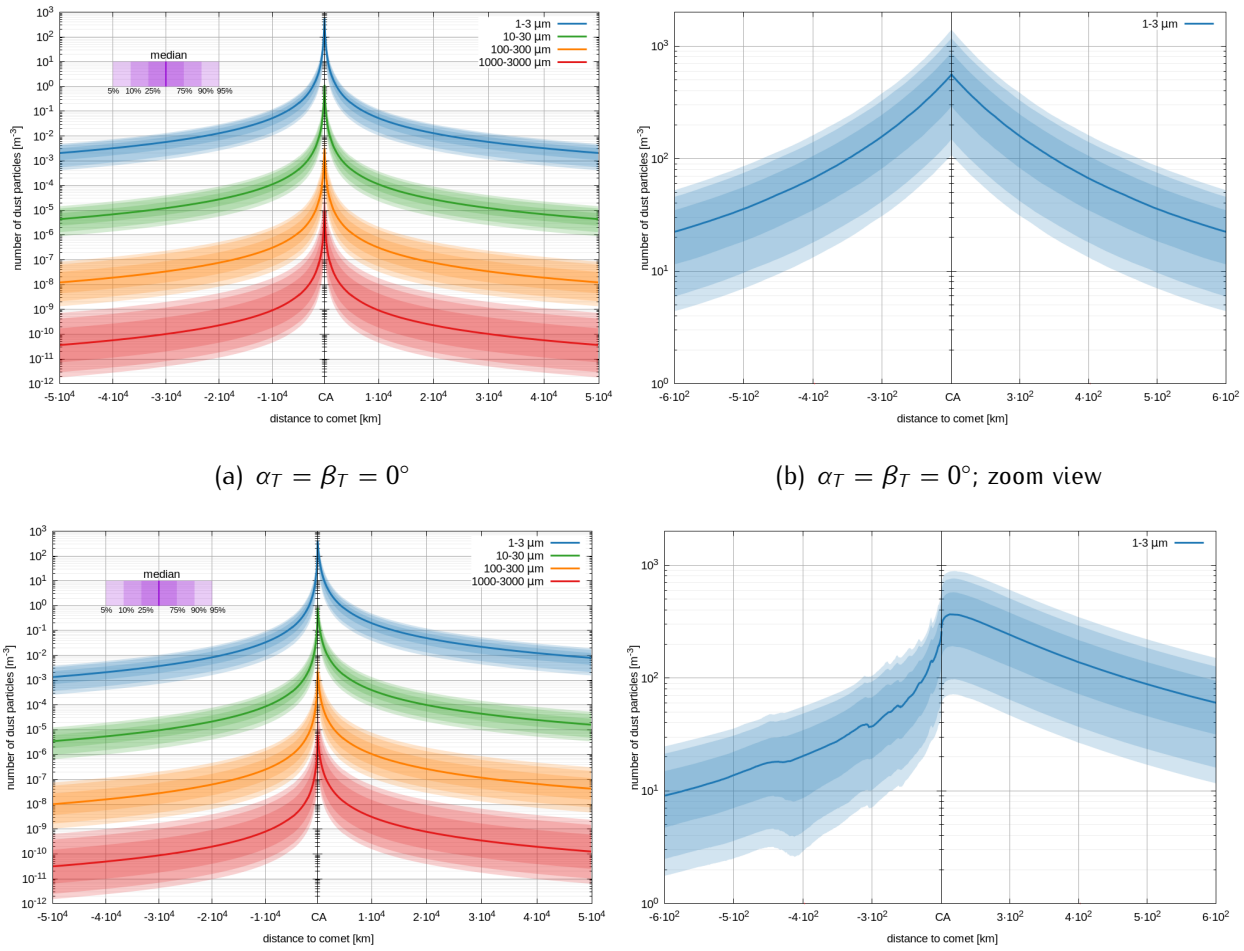

(a) $\alpha_T = \beta_T = 0°$

(b) $\alpha_T = \beta_T = 0°$; zoom view

(c) $\alpha_T = 0°; \beta_T = 60°$

(d) $\alpha_T = 0°; \beta_T = 60°$; zoom view

FIG. 13. Number densities as a function of cometo centric distance for S/C B2 for different dust sizes.

inherent to the EDCM. We can therefore use the rough empirical relation

$$N_{col}(\alpha_T) = N_{col}(0)\cos^{0.8}(\alpha_T) \tag{6}$$

to scale the nominal results to different values of α_T.

Finally, we varied β_T (β in Fig. 8) which not only changes the phase angle at CA to β_T (if $\alpha_T = 0°$) but also skews the trajectory such that the asymptotic phase angles are $90 \pm \beta_T$. If $\alpha_T = 0°$, as assumed here, the S/C will usually go through zero phase shortly after/before CA. Figure 12 b) shows the normalised column density to the values of each dust sizes column density at $\beta_T = 0°$ as well as the size averaged relative column density. The dependency of the column density on β_T is weaker than that of α_T. The maximum decrease,at $\beta_T = 60°$, is

$\sim 15\%$. We can use the rough empirical relation

$$N_{col}(\beta_T) = N_{col}(0)\cos^{0.24}(\beta_T) \tag{7}$$

to scale the nominal results to different values of β_T.

But the change in β_T will result in an asymmetric dust distribution along the S/C trajectory. This is illustrated for S/C B2 in Fig. 13 showing the examples where β_T is 0° (top row) and 60° (bottom row). In the case where $\beta_T = 60°$ the inbound densities are lower than for the symmetric trajectory because the inbound asymptotic phase angle is 150° instead of 90°. Conversely, the outbound densities are higher than for the symmetric trajectory because the outbound asymptotic phase angle is 30° instead of 90°. Further the maximum number density will occur shortly after CA instead of at CA.

Finally, we should state that all changes in the CA distance, α_T, and β_T result in small changes in the column densities compared to the inherent uncertainties resulting from our knowledge of the input parameters.

VI. SCALING OF RESULTS TO OTHER DUST SIZES OR BIN INTERVALS

In the case that the model does not provide the results for the desired dust radius or size of the dust bin (by default half a decade) we provide a simple scaling. We should caution the user to use these scaling with caution as they might break down if pushed to their extremes (e.g. to very short size intervals). All scaling we provide here apply only to the respective median cases of the column density of the respective spacecraft.

First we will define some general functions to calculate the respective scaling later on. The column density as a function of the dust radius, a, follows a double asymptotic power law of the form

$$N_{col,fit}(a) = C_1 a^{-\beta_1} + C_2 a^{-\beta_2} \quad , \tag{8}$$

where β_i are the respective asymptotic power law exponents, and

$$C_i(a_{0,i}, N_{0,i}, \beta_i) = N_{0,i} a_{0,i}^{\beta_i} \tag{9}$$

is the normalisation constant given where $N_{0,i}$ is the column density at reference size $a_{0,i}$. The values of these parameters for the three spacecraft are given in Table IV.

TABLE IV. Parameters for interpolation between dust sizes and bin interval lengths.

S/C	$a_{0,1}$	$N_{0,1}$	β_1	$a_{0,2}$	$N_{0,2}$	β_2
A		1.5E7			4.1E-6	
B1	1E-6 m	3.0E7	3	1E-1 m	8.2E-6	2.48
B2		1.5E8			4.1E-5	

Next we define the length of our dust size bins as

$$\Delta a = 10^d \quad , \tag{10}$$

where d is a decade fraction, e.g. 0.5 for half a decade or 0.25 for a quarter decade. From this it follow that a specific dust bin starting at a will extend to $a \cdot \Delta a$.

A. Interpolation between dust bins

To interpolate the results from one dust bin radius to another while keeping the length of the dust bin (a) unchanged we can proceed in the following manner. When the target dust size is a_t we lookup the dust bin size, a_r, which is just smaller than our target size. This reference dust bin, a_r, has a certain column density, $N_{col}(a_r)$, according to the EDCM. Using Eq. 8 the column density for our target size, a_t (covering the dust range from a_t to $a_t \cdot \Delta a$), will be

$$N_{col}(a_t) = N_{col}(a_r)\frac{N_{col,fit}(a_t)}{N_{col,fit}(a_r)} \quad . \tag{11}$$

B. Interpolation of dust bin length

Next we discuss how the length of the dust bins can be changed. The results of the EDCM are provided for bins with a length of half a decade in dust radius. If one wants to know the results for a bin size of a quarter decade instead of a half a decade the following procedure can be applied. We should caution the reader at this point that we have tested this scaling only down to a quarter decade. While we believe that it also holds for smaller intervals the user should be aware of this limitation and that smaller bin lengths could be associated with additional uncertainty.

The provided solution have dust bin lengths which are half a decade in dust radius. Or according to Eq. 10 this means that our reference decade fraction is $d_r = 0.5$. The target decade fraction shall be d_t. First we define the helper function

$$H(a_0, N_0, \beta, d, a) = \frac{C(a_0, N_0, \beta)}{(1-\beta)} a^{1-\beta} \left(10^{d(1-\beta)} - 1\right) \quad , \tag{12}$$

which allows us to calculate the integral, I, of Eq. 8 for one dust bin:

$$I(a_{0,1}, N_{0,1}, \beta_1, a_{0,2}, N_{0,2}, \beta_2, d, a) = H(a_{0,1}, N_{0,1}, \beta_1, d, a) + H(a_{0,2}, N_{0,2}, \beta_2, d, a) \quad . \tag{13}$$

From this we can now calculate the scaling constant, S, for a bin that was initially covered the decade fraction d_r to one that covers the decade fraction d_t. This scaling constant can be written as

$$S(a_{0,1}, N_{0,1}, \beta_1, a_{0,2}, N_{0,2}, \beta_2, \mathbf{d_r}, \mathbf{d_t}, a) = \frac{I(a_{0,1}, N_{0,1}, \beta_1, a_{0,2}, N_{0,2}, \beta_2, \mathbf{d_t}, a)}{I(a_{0,1}, N_{0,1}, \beta_1, a_{0,2}, N_{0,2}, \beta_2, \mathbf{d_r}, a)} \quad . \tag{14}$$

The column density of the new bin length, $N_{col}(a, d_t)$, can now be calculated from the column density given by the EDCM, $N_{col}(a, d_r)$:

$$N_{col}(a, \mathbf{d_t}) = N_{col}(a, \mathbf{d_r}) \cdot S(a_{0,1}, N_{0,1}, \beta_1, a_{0,2}, N_{0,2}, \beta_2, \mathbf{d_r}, \mathbf{d_t}, a) \quad . \tag{15}$$

Though we have kept all equations general, we remind the reader that currently $d_r = 0.5$.

VII. OUTPUT FORMAT

The output files of version ZZZ are placed in the following folder structure

- **figures** (contains additional figures not included in the documentation)
  - **supplement** (contains supplementary figures related to the supplementary data)
- **scXX** (contains all data for S/C XX, where XX ∈ [A, B1, B2])
  - **colDen** (contains the files with the dust column densities integrated along the S/C trajectory)
    File names: *r_colDen_scXX_vZZZ.dat*
  - **numDen** (contains the files with the local dust number densities along the S/C trajectory)

    * **YY** (contains results for the dust bin YY, where YY ∈ [21, 26, 31, 36, 41, 46, 51, 56, 61, 66, 71]; which dust bin corresponds to which size can be found in Tab. V)
      File names: *r_numDen_YY_scXX_vZZZ.dat*

- **supplement** (contains the supplementary data: comparison of with Giotto data (Sec. IV), and the sensitivity study (Sec. V))

  – **SCTN** (contains all data for S/C trajectory SCTN, where SCTN ∈ [Giotto, scB2_alpha=00_beta=15, scB2_alpha=00_beta=30, scB2_alpha=00_beta=45, scB2_alpha=00_beta=60, scB2_alpha=15_beta=00, scB2_alpha=30_beta=00, scB2_alpha=45_beta=00, scB2_alpha=60_beta=00])
    NOTE: *The Giotto folder contains a special version of the model (v4.0-Halley) which covers only a narrow part of parameter space to mimic as closely as possible comet 1P/Halley and is thus not the nominal case to be used but was intended solely for the comparison with Giotto data and validation of the model (see Sec. IV).*

    * **colDen** (contains the files with the dust column densities integrated along the S/C trajectory)
      File names: *r_colDen_SCTN_vZZZ.dat*
    * **numDen** (contains the files with the local dust number densities along the S/C trajectory)
      · **YY** (contains results for the dust bin YY, where YY ∈ [21, 26, 31, 36, 41, 46, 51, 56, 61, 66, 71]; which dust bin corresponds to which size can be found in Tab. V)
        File names: *r_numDen_YY_SCTN_vZZZ.dat*

A. Column density files

The column density files (*r_colDen_scXX_vZZZ.dat*) contain one row per dust size bin. The file has 12 columns containing the following information:

- **1st column:** dust bin id

- **2^{nd} column:** lower boundary of the dust bin, a_{min} [m], see Tab. V for upper bound.

- **3^{rd}-11^{th} column:** 50^{th}, 25^{th}, 75^{th}, 10^{th}, 90^{th}, 5^{th}, 95^{th}, 1^{st}, and 99^{th} percentiles of the dust column density integrated along the S/C trajectory [m^{-2}]

- **13^{th} column:** number of cases run

TABLE V. Legend for which dust bin id, YY, corresponds to which dust size range. The results of dust bin YY correspond to the respective integrated quantities in the dust radius range from a_{min} to a_{max}

bin id	a_{min} [m]	a_{max} [m]
21	$1.00 \cdot 10^{-6}$	$3.16 \cdot 10^{-6}$
26	$3.16 \cdot 10^{-6}$	$1.00 \cdot 10^{-5}$
31	$1.00 \cdot 10^{-5}$	$3.16 \cdot 10^{-5}$
36	$3.16 \cdot 10^{-5}$	$1.00 \cdot 10^{-4}$
41	$1.00 \cdot 10^{-4}$	$3.16 \cdot 10^{-4}$
46	$3.16 \cdot 10^{-4}$	$1.00 \cdot 10^{-3}$
51	$1.00 \cdot 10^{-3}$	$3.16 \cdot 10^{-3}$
56	$3.16 \cdot 10^{-3}$	$1.00 \cdot 10^{-2}$
61	$1.00 \cdot 10^{-2}$	$3.16 \cdot 10^{-2}$
66	$3.16 \cdot 10^{-2}$	$1.00 \cdot 10^{-1}$
71	$1.00 \cdot 10^{-1}$	$3.16 \cdot 10^{-1}$

B. Number density files

The number density files (*r_numDen_YY_scXX_vZZZ.dat*) contain 12 columns with the following information:

- **1^{st} column:** Distance from the S/C to the comet [m]. Negative values indicate pre-CA, whilst positive values indicate post-CA.

- **2^{nd} column:** Phase angle [°]. Negative values indicate pre-CA, whilst positive values indicate post-CA.

- **3^{rd}-11^{th} column:** 50^{th}, 25^{th}, 75^{th}, 10^{th}, 90^{th}, 5^{th}, 95^{th}, 1^{st}, and 99^{th} percentiles of the local dust number density at the specific point along the S/C trajectory [m^{-3}]

- **13^{th} column:** number of cases run

C. Conversion from radius to mass

Though all results are presented as a function of dust radius, a, they can be converted to mass, m_d, using the average bulk dust density, $\bar{\varrho}_d$, of all cases of the respective version:

$$m_d(a) = \frac{4\pi}{3} a^3 \bar{\varrho}_d \quad . \tag{16}$$

The average bulk dust density of each version is given in table VI. Though this is a simplification, the error stemming from that is much smaller than the overall uncertainties of the model. Importantly, the number densities and column densities are presented per half decade in dust radius. Hence the conversion from radius to mass results in densities per 1.5 decades in mass.

TABLE VI.

version	$\bar{\varrho}_d$ [kg m^{-3}]
1.1	457
2.1	452
3.0	543
4.0	570

LIST OF ACRONYMS

CI Comet Interceptor

EDCM Engineering Dust Coma Model

α phase angle

α_T trajectory angle in the meridional plane

β differential power law exponent of the dust size distribution

β_T trajectory angle in the equatorial plane

χ dust-to-gas mass production rate ratio

$\phi(\alpha)$ dust phase function

ρ_N bulk density of the nucleus

φ solar zenith angle

ϱ_d bulk density of the dust particles

$\vec{r}$ nucleo-centric radius-vector ($r = |\vec{r}|$)

a radius of dust particles

I brightness of the dust coma

m_d mass of dust particles

N column density of dust particles [m^{-2}]

n number density of dust particles [m^{-3}]

$q(\varphi)$ gas emission distribution

$q_g^{180^\circ}/q_g^{0^\circ}$ relative night side activity

Q_g^{equiv} global gas production rate for an equivalent sphere nucleus with $R_N = 1$ km

$q_{rad}(a)$ radiation pressure efficiency

$q_{sca}(a)$ scattering efficiency

R_N radius of the nucleus

T_N nucleus temperature at the sub-solar point

x, y, z cartesian frame with origin in the centre of mass of the nucleus and x-axis directed to the Sun.

CA closest approach

ACKNOWLEDGEMENTS

This document has been made with contributions from:
Vladimir Zakharov — INAF-IAPS, Italy
Raphael Marschall — Southwest Research Institute, USA
Cecilia Tubiana — INAF-IAPS, Italy
Michael S. P. Kelley — University of Maryland, USA
Jessica Agarwal — Technische Universität Braunschweig, Germany
Vincenzo Della Corte — INAF-IAPS, Italy
Stavro Ivanovski — INAF Astronomical Observatory of Trieste, Italy
Fernando Moreno — Instituto de Astrofisica de Andalucia, CSIC, Spain
Olga Muñoz — Instituto de Astrofísica de Andalucía, CSIC, Spain
Frank Postberg — Freie Universität Berlin, Germany
Alessandra Rotundi — Università degli Studi di Napoli "Parthenope", Italy
Jean-Baptiste Vincent — DLR Institute for Planetary Research, Germany

[1] M. F. A'Hearn, R. C. Millis, D. O. Schleicher, D. J. Osip, and P. V. Birch, The ensemble properties of comets: Results from narrowband photometry of 85 comets, 1976-1992., Icarus **118**, 223 (1995).

[2] R. Marschall, J. Markkanen, S.-B. Gerig, O. Pinzón-Rodríguez, N. Thomas, and J.-S. Wu, The dust-to-gas ratio, size distribution, and dust fall-back fraction of comet 67P/Churyumov-Gerasimenko: Inferences from linking the optical and dynamical properties of the inner comae., Frontiers in Physics **8**, 227 (2020), arXiv:2005.13700 [astro-ph.EP].

[3] V. V. Zakharov, A. V. Rodionov, M. Fulle, S. L. Ivanovski, N. Y. Bykov, V. Della Corte, and A. Rotundi, Practical relations for assessments of the gas coma parameters, Icarus **354**, 114091 (2021).

[4] V. V. Zakharov, S. L. Ivanovski, J. F. Crifo, V. Della Corte, A. Rotundi, and M. Fulle, Asymptotics for spherical particle motion in a spherically expanding flow, Icarus **312**, 121 (2018).

[5] R. Marschall, C. C. Su, Y. Liao, N. Thomas, K. Altwegg, H. Sierks, W. H. Ip, H. U. Keller, J. Knollenberg, E. Kührt, I. L. Lai, M. Rubin, Y. Skorov, J. S. Wu, L. Jorda, F. Preusker, F. Scholten, A. Gracia-Berná, A. Gicquel, G. Naletto, X. Shi, and J. B. Vincent, Modelling observations of the inner gas and dust coma of comet 67P/Churyumov-Gerasimenko using ROSINA/COPS and OSIRIS data: First results, A&A **589**, A90 (2016).

[6] J. Markkanen, J. Agarwal, T. Väisänen, A. Penttilä, and K. Muinonen, Interpretation of the Phase Functions Measured by the OSIRIS Instrument for Comet 67P/Churyumov-Gerasimenko, ApJ **868**, L16 (2018), arXiv:1811.03899 [astro-ph.EP].

[7] S. B. Gerig, R. Marschall, N. Thomas, I. Bertini, D. Bodewits, B. Davidsson, M. Fulle, W. H. Ip, H. U. Keller, M. Küppers, F. Preusker, F. Scholten, C. C. Su, I. Toth, C. Tubiana, J. S. Wu, H. Sierks, C. Barbieri, P. L. Lamy, R. Rodrigo, D. Koschny, H. Rickman, J. Agarwal, M. A. Barucci, J. L. Bertaux, G. Cremonese, V. Da Deppo, S. Debei, M. De Cecco, J. Deller, S. Fornasier, O. Groussin, P. J. Gutierrez, C. Güttler, S. F. Hviid, L. Jorda, J. Knollenberg, J. R. Kramm, E. Kührt, L. M. Lara, M. Lazzarin, J. J. Lopez Moreno, F. Marzari, S. Mottola, G. Naletto, N. Oklay, and J. B. Vincent, On deviations from free-radial outflow in the inner coma of comet 67P/Churyumov-Gerasimenko, Icarus **311**, 1 (2018).

[8] D. G. Schleicher and A. N. Bair, Chemical and Physical Properties of Comets in the Lowell Database: Results from Four Decades of Narrowband Photometry, in

AAS/Division for Planetary Sciences Meeting Abstracts #48, AAS/Division for Planetary Sciences Meeting Abstracts, Vol. 48 (2016) p. 308.04.

[9] I. Bertini, F. La Forgia, C. Tubiana, C. Güttler, M. Fulle, F. Moreno, E. Frattin, G. Kovacs, M. Pajola, H. Sierks, C. Barbieri, P. Lamy, R. Rodrigo, D. Koschny, H. Rickman, H. U. Keller, J. Agarwal, M. F. A'Hearn, M. A. Barucci, J. L. Bertaux, D. Bodewits, G. Cremonese, V. Da Deppo, B. Davidsson, S. Debei, M. De Cecco, E. Drolshagen, S. Ferrari, F. Ferri, S. Fornasier, A. Gicquel, O. Groussin, P. J. Gutierrez, P. H. Hasselmann, S. F. Hviid, W. H. Ip, L. Jorda, J. Knollenberg, J. R. Kramm, E. Kührt, M. Küppers, L. M. Lara, M. Lazzarin, Z. Y. Lin, J. J. L. Moreno, A. Lucchetti, F. Marzari, M. Massironi, S. Mottola, G. Naletto, N. Oklay, T. Ott, L. Penasa, N. Thomas, and J. B. Vincent, The scattering phase function of comet 67P/Churyumov-Gerasimenko coma as seen from the Rosetta/OSIRIS instrument, **469**, S404 (2017).

[10] K. Wilhelm, Rotation and precession of comet Halley, Nature (London) **327**, 27 (1987).

[11] D. Krankowsky, P. Lammerzahl, I. Herrwerth, J. Woweries, P. Eberhardt, U. Dolder, U. Herrmann, W. Schulte, J. J. Berthelier, J. M. Illiano, R. R. Hodges, and J. H. Hoffman, In situ gas and ion measurements at comet Halley, Nature (London) **321**, 326 (1986).

[12] H. U. Keller, W. A. Delamere, H. J. Reitsema, W. F. Huebner, and H. U. Schmidt, Comet P/Halley's nucleus and its activity, A&A **187**, 807 (1987).

[13] H. Rickman, The nucleus of comet Halley: Surface structure, mean density, gas and dust production, Advances in Space Research **9**, 59 (1989).

[14] J. A. M. McDonnell, G. S. Pankiewicz, P. N. W. Birchley, S. F. Green, and C. H. Perry, The In-Situ Particulate Size Distribution Measured for One Comet: P/Halley, Analysis of Returned Comet Nucleus Samples (1997).

[15] C. Snodgrass and G. H. Jones, The European Space Agency's Comet Interceptor lies in wait, Nature Communications **10**, 5418 (2019).

[16] T. I. Gombosi and M. Horanyi, Time-dependent Numerical Modeling of Dust Halo Formation at Comets, Astrophys. J. **311**, 491 (1986).